analytical chemistry

Article

pubs.acs.org/ac

Quantum Dot/Carrier–Protein/Haptens Conjugate as a Detection Nanobioprobe for FRET-Based Immunoassay of Small Analytes with All-Fiber Microfluidic Biosensing Platform

Feng Long,[†,‡] Chunmei Gu,[†] April Z. Gu,[§] and Hanchang Shi*[,†]

[†]State Key Joint Laboratory of ESPC, School of Environment, Tsinghua University, Beijing 100084, People's Republic of China

[‡]Department of Chemistry, Massachusetts Institute of Technology, Cambridge, Massachusetts 02139, United States

[§]Department of Civil and Environmental Engineering, Northeastern University, Boston, Massachusetts 02115, United States

Supporting Information

ABSTRACT: This study demonstrates the use of carrier-protein/haptens conjugate (e.g., BSA/2,4-dichlorophenoxyacetic acid, 2,4-D-BSA) for biological modification of quantum dots (QDs) for the detection of small analytes. Bioconjugated QDs, which are used as a detection nanoimmunoprobe, were prepared through conjugating carboxyl QDs with 2,4-D-BSA conjugate. Based on the principle of quantum dot–fluorescence resonance energy transfer (QD-FRET), an all-fiber microfluidic biosensing platform has been developed for investigating FRET efficiency, immunoassay mechanism and format, and binding kinetics between QD immunoprobe and fluorescence labeled anti-2,4-D monoclonal antibody. The structure of multiplex-haptens/BSA conjugate coupling to QD greatly improves the FRET efficiency and the sensitivity of the nanosensor. With a competitive detection mode, samples containing different concentrations of 2,4-D were incubated with a given concentration of QD immunoprobe and fluorescence-labeled antibody, and then detected by the all-fiber microfluidic biosensing platform. A higher concentration of 2,4-D led to less fluorescence-labeled anti-2,4-D antibody bound to the QD immunoprobe surface and, thus, a lower fluorescence signal. The quantification of 2,4-D over concentration ranges from 0.5 nM to 3 μM with a detection limit determined as 0.5 nM. The performance of the nanosensor with spiked real water samples showed good recovery, precision, and accuracy, indicating that it was less suspectable to water matrix effects. With the use of different QD nanobioprobes modified by other carrier-protein/haptens conjugates, this biosensing protocol based on QD-FRET can be potentially applied for on-site, real-time, inexpensive, and easy-to-use monitoring of other trace analytes.

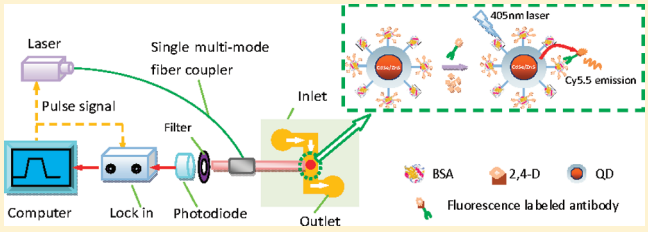

Most of the analytes of environmental interest, such as pesticides, persistent organic pollutants (POPs), endocrine-disrupting chemicals (EDCs), explosives, and toxins, possess a molecular weight of <1 kDa, and they cause many severe health problems at very low concentrations.[1−3] Until recently, the quantification of small analytes has been limited to the traditional chromatographic and spectroscopic technologies. These methods, although accurate with low detection limits, are labor-intensive and require expensive and sophisticated instrumentation, as well as complicated and multistep sample preparation, which prohibits potential real-time and on-site practical applications. Therefore, considerable research interests have risen for detecting low levels of small molecules in biosensor developments. Among them, nanoparticle (NP)-based biosensors have gained great attention, because of their simplicity, robustness, sensitivity, specificity, and cost-effectiveness.[4] NP-based biosensors can usually carry out analyte recognition and binding, as well as convert the biorecognition event to a measurable optical or electric signal through an integrated signal transduction system.[4]

Nanometer-sized quantum dots (QDs) have emerged as promising alternative bioanalytical tools, because of their unique optical properties, including high quantum yield, photostability, narrow emission spectrum, and broad absorption.[5,6] The narrow, size-tuned, and symmetric emission spectra of QDs have made them excellent donors for fluorescence resonance energy transfer (FRET) sensors, and they greatly reduce the overlap between the emission spectra of donor and acceptor and circumvents the cross-talk in such FRET pairs.[5,6] Meanwhile, QDs have broad excitation spectra as donors, and they allow excitation at a single wavelength far removed (>100 nm) from their respective emissions, which can avoid the direct excitation of the acceptor. In addition, the high photobleaching threshold and good chemical stability of QDs greatly improve the detection sensitivities and detection limits.[6,7] Therefore, QD-based FRET biosensors have been widely used in immunoassay,[7,8] medical imaging,[9,10] clinical/diagnostic as-

Received: January 5, 2012
Accepted: March 20, 2012
Published: March 20, 2012

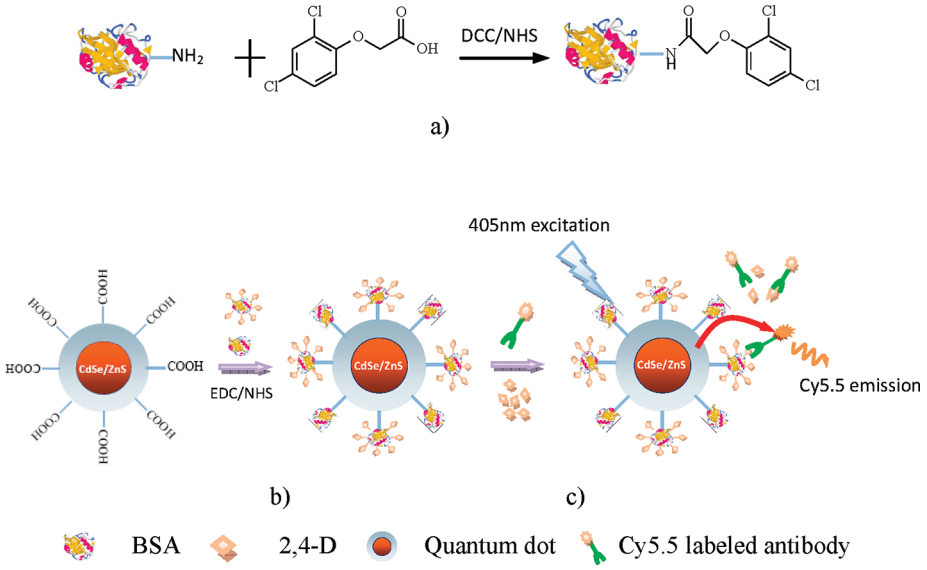

Figure 1. Preparation of QD/carrier−protein/haptens nanoimmunoprobe and immunoassay mechanism for the detection of 2,4-D: (a) synthesis of 2,4-D-BSA conjugates and (b) synthesis of QD/2,4-D-BSA immunoprobe. (c) Depiction of the competitive immunoassay mechanism of 2,4-D based on QD-FRET.

says,[11] and biomolecular binding assay.[12] Antibody bioconjugates of QDs, prepared using covalent or noncovalent linking approaches, are the most developed and widespread detection bioprobes to integrating QDs into bioanalyses.[7,8,13] However, the control over the number of antibodies per QD and their orientation and position relative to the QD is very difficult. Because of the possibility of inadvertently disrupting the binding site when conjugating QD with antibody, the activity loss of antibody is inevitable.[6,11,14] In addition, antibodies usually must be cryopreserved, but QDs cannot be frozen, which makes storage of the QD antibody a major obstacle for its practical applications.

To effectively address these challenges, we have developed carrier−protein−haptens-coupled QD nanobioprobe protocols to perform rapid and sensitive detection of small targets in real water samples. 2,4-Dichlorophenoxyacetic acid (2,4-D, MW = 221.04), one of the most widely used pesticides worldwide,[15] was selected as a model target. 2,4-D has been shown to lead to cancer in humans,[16] endocrine-disrupting activities,[15,17] and degenerative changes in the nervous system.[18] QD nanoimmunoprobes were prepared by conjugating carboxyl QDs with a 2,4-D-BSA conjugate, which is regarded as the immunological recognition of the anti-2,4-D antibody, as well as being used for optical transduction. To improve upon existing immunoassay techniques (e.g., ELISA, SPR, and microarray) based on static solid/liquid interface reaction, regarding their sensitivity, overall analysis time, and simplified manipulation, an all-fiber microfluidic biosensing platform has been developed. The ambulatory fluid is expected to accelerate the reaction among analytes, the fluorescence-labeled antibody, and the QD-BSA-2,4-D nanoconjugate, as well as prevent QDs from nonspecific deposition at surfaces. The binding kinetics of the QD-BSA-2,4-D immunoprobe and the fluorescence-labeled anti-2,4-D monoclonal antibody, and the sensitivity and selectivity of this nanoimmunosensor, based on QD-FRET, have also been evaluated.

EXPERIMENTAL SECTION

Materials. Bovine serum albumin (BSA), 2,4-dichlorophenoxyacetic acid (2,4-D), 2,4-dichlorophenol (2,4-DCP), 4-(2,4-dichlorophenoxy)butyric acid (2,4-DB), 2,4,5-trichlorophenoxyacetic acid (2,4,5-T), 4-chlorophenoxyacetic acid (CPA), 4-chloro-*o*-tolyloxyacetic acid (MCPA), 1-ethyl-3-(3-dimethylamino-propyl) carbodiimide hydrochloride (EDC), *N*,*N*′-dicyclohexylcarbodiimide (DCC), and *N*-hydroxysuccinimide (NHS) were purchased from Sigma−Aldrich (Steinheim, Germany). All solutions were prepared with ultrapure water from a Millipore Milli-Q sytem. All the other reagents, unless specified, were supplied by the Beijing Chemical Agents (China). All chemicals were of analytical reagent (AR) grade.

Qdot 605 ITK carboxyl quantum dots were obtained from Invitrogen, Ltd. (USA). Transmission electron microscopy (TEM) (Model H-7650B, Hitachi, Japan) images revealed that the Qdots were uniform in size, and only the inorganic particles are directly visualized at ∼10 nm × 5 nm (see Figure S-1a in the Supporting Information). The size of the polymer-capped QDs (∼9−15 nm) was also characterized by dynamic laser scattering (DLS) (see Figure S-1b in the Supporting Information)

Dye Cy5.5 labeled monoclonal anti-2,4-D antibody (Reference No. 2H8) were produced by our research group.[19] The affinity and specificity of the produced monoclonal antibodies to 2,4-D were characterized in conjugate-coated ELISA formats. The hapten−carrier conjugate 2,4-D-BSA was prepared by conjugating an amine of BSA to 2,4-D through the DCC/NHS chemistry, which is described as follows (Figure 1a). 2,4-D (22.0 mg) and NHS (11.5 mg) were dissolved in 2 mL of dimethyl formamide (DMF), and then activated by dropwise adding 20.6 mg of DCC. The mixture was stirred at room temperature for 18 h and then centrifugated at 5000 rpm. The supernatant was added drop by drop to create a 30-mL volume of 5 mg/mL BSA solution for conjugation. The reaction mixture was then dialyzed at 4 °C and lyophilized to get the conjugates. The estimated number of hapten molecules attached to the carrier protein (hapten to protein molar ratio, MR) BSA, determined by matrix-assisted laser desorption

dx.doi.org/10.1021/ac3000495 | *Anal. Chem.* 2012, 84, 3646−3653

ionization−time of flight (MALDI-TOF) mass spectroscopy (MS), was 12, as described previously.[19,20]

Preparation of Quantum Dots Nanoimmunoprobe. The QD-2,4-D-BSA nanoconjugate was prepared by conjugating an amine of BSA to commerical carboxyl-coated Qdot 605 through the EDC/sulfo-NHS chemistry (Figure 1b). The EDC and Sulfo-NHS reagents were used together, to enhance the conjugation efficiency. Fifty microliters (50 μL) of 8 μM stock solution of carboxyl QDs were diluted to 0.5 mL using a 10 mM borate buffer (pH 7.4), and 0.5 mL of a 3 mg/mL 2,4-D-BSA was added. After being well-mixed, 10 μL of a 10 mg/mL as-prepared EDC/NHS solution was added to the mixture, which was gently stirred for 1.5 h at room temperature for the conjugation. To block the unreacted carboxyl sites on the QD surface, 0.5 mL of 10 mg/mL BSA was added to the mixture and reacted for an additional 1 h. The mixture then was filtered through a 0.2 μm PES syringe filter to remove any large aggregates before being transferred to a clean centrifugal ultrafiltration unit (100 kDa cutoff; GE Healthcare, USA). To remove any excess unbound protein, this solution was centrifuged at 3000 rpm for the ultrafiltration unit for five buffer exchanges (50 mM borate buffer, pH 8.3). After completing ultracentrifugation, the solution was filtered through a 0.2 μm syringe filter to remove any aggregates. The products were stored at 4 °C before use. The quantification of the QD immunoprobe prepared was determined as described elsewhere.[21]

Instrumentation: Development of the All-Fiber Microfluidic Biosensing Platform. A portable all-fiber microfluidic biosensing platform (32 cm × 28 cm × 16 cm, weighing ∼10 lbs) was developed and shown in Figure 2. (For more information, see Figure S-2 in the Supporting Information). In this system, the 405-nm 20 mW pulse diode laser (HuayuanStar, Ltd., China) with a pigtail is selected as the excited light resource for its monochrome, stability, and compactness. The laser beam from the diode laser was directly launched into the single-mode fiber of the single multimode silica fiber-optic coupler. The laser light then entered the multimode fiber with a diameter of 600 μm and numerical aperture of 0.22 from the single-mode fiber. Meanwhile, this multimode fiber was used to collect the fluorescence excited by laser light. Instead of using various optical separation components (e.g., lens, dichroic mirror), a single−multi fiber-optic coupler provides for the transmission of the excitation light and the collection and transmission of the fluorescence in this system. Because of the reduced optical components and no-longer-required optical alignment, light transmission efficiency is higher, light loss is lower, and the S/N ratio is improved. An ∼10 mW output can be obtained from the distal end of a multimode fiber, which directly excited the QDs in the glass microfluidic channel (600 μm × 100 μm) (Shanghai Wenchang Chip Technology Co., Ltd., China). The emission signal of Cy5.5 dye labeled on excited anti-2,4-D antibodies then was collected by the multimode optical fiber and filtered by means of a bandpass filter (FF01-710/40, Semrock, USA) and detected by photodiodes through a digital lock-in amplifier that was interfaced to a mini-computer.

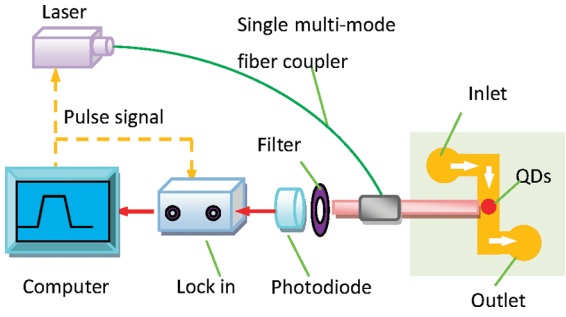

Figure 2. Schematic of the all-fiber microfluidic biosensing platform.

Optimization of Competitive Immunological Reaction. The binding reaction kinetics between the QD immunoprobe and the fluorescence-labeled anti-2,4-D antibody was first tested. To obtain the binding kinetics curve, a 100-μL sample cell instead of the microfluidic channel was used in the all-fiber biosensing platform system, in which a volume of 80 μL 1 × PBS (0.01 mol/L), ∼2 nM QD immunoprobe was suspended. In the next step, 10 nM fluorescence labeled antibody was added at room temperature, and the mixture was subjected to detection of the all-fiber biosensing platform. The time point of addition of the antibody was regarded as time zero, and the kinetics plot was obtained by recording fluorescence against time. From this, the optimizal detection time of 2,4-D can be determined. Then, two assay formats were compared: fluorescence-labeled anti-2,4-D antibody and QD immunoprobe are first incubated and 2,4-D solution is then added, or fluorescence-labeled anti-2,4-D antibody and 2,4-D solution are first incubated and QD immunoprobe is then added.

In addition, reagent concentrations of the QD immunoprobe (1.0−4.0 nM) and fluorescence-labeled antibody (2.0−20 nM) were optimized to investigate the best experimental conditions for competitive immunological recognition and further generation of the fluorescence signal. A sensitivity index (F/F_0), which is the ratio between the fluorescence signal obtained in the presence of the analyte (F) and the signal in the absence of analyte (F_0), was introduced to determine the optimum experimental conditions.

Competitive Fluorescence Immunoassay of 2,4-D. Standard 2,4-D solutions were prepared via serial dilution with 1 × PBS, in a range of 10 nM to 30 μM. After an addition of 5 nM fluorescence-labeled antibody, the mixture were then incubated with 1.5 nM QD immunoprobe for 5 min at room temperature. The mixture was then introduced to the microfluidic channel. After excitation (λ_{ex} = 405 nm), the final stage of the assay involved the fluorescence measurement of Cy5.5 using the all-fiber biosensing platform.

To assess the selectivity of the sensor, its responses to such potentially interfering materials as 2,4,5-T, 2,4-DCP, 2,4-DB, CPA, and MCPA at concentrations up to 30 μM were evaluated. To evaluate potential environmental sample matrix effects on 2,4-D detection, spiked samples of bottled water, laboratory tap water, the advanced treatment effluent water (Qinghe Wastewater Plant, Beijing), and Beihai Lake (Beijing) were tested at concentrations of 20, 200, and 1000 nM.

RESULTS AND DISCUSSION

Preparation and Characterization of QD Immunoprobe. Covalent immobilization of the 2,4-D-BSA conjugate on the carboxyl-coated QD surface was achieved using the EDC/NHS coupling strategy. After conjugation, TEM bright-field images revealed that Qdots were still uniform in size, and negative staining of the conjugates reveals an additional halo, which is consistent with the conjugation of protein to the particles (see Figure S-1c in the Supporting Information). To

dx.doi.org/10.1021/ac3000495 | Anal. Chem. 2012, 84, 3646−3653

evaluate whether there was any difference in the photoluminescence (PL) emission spectrum of Qdots after conjugation to 2,4-D-BSA, PL measurements of Qdots were performed using a Hitachi Model F-7000 fluorescence spectrophotometer (Japan) with 365-nm excitation light. The spectrum of bioconjugated Qdot 605 is still symmetrical and almost identical to that of commercial Qdots, with only a slight red shift (Figure S-3 in the Supporting Information), and maximum emission wavelengths are 605.0 and 606.0 nm for commercial Qdot 605 (black line) and 2,4-D-BSA conjugated Qdot 605 (Red line), respectively.

To confirm that the observed fluorescence signal was from the fluorescence resonance energy transfer between the QD immunoprobe and the fluorescence-labeled anti-2,4-D antibody, we conducted several control experiments, whose results are shown in Figure 3 (each curve being the average of three

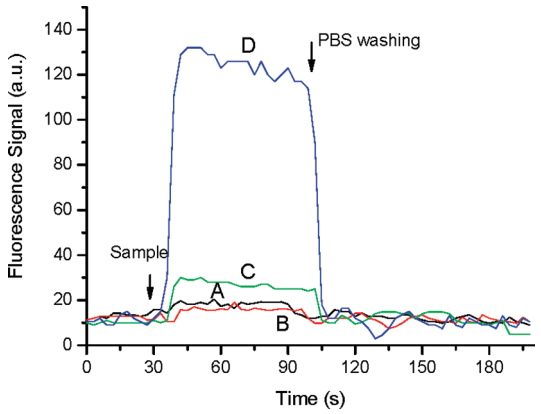

Figure 3. Sensor's performance and responses to various controls: 4 nM QD immunoprobe (trace A); 10 nM fluorescence-labeled rabbit-anti mouse antibody and 2 nM QD immunoprobe (trace B); 1 nM fluorescence-labeled anti-2,4-D antibody and 2 nM QD immunoprobe (trace C); and 10 nM fluorescence-labeled anti-2,4-D antibody and 2 nM QD immunoprobe (trace D).

independent curves). First, 4 nM of QD immunoprobe was directly delivered into the microfluidic channel and a small fluorescence signal was observed, which originated from the fluorescence of excited QD and most of them were effectively filtered by the bandpass filter in the system. Second, 10 nM of fluorescence-labeled rabbit-anti mouse antibody and 2 nM of QD immunoprobe was incubated for 5 min and then delivered into the microfluidic channel, but no obvious fluorescent signal was observed, thereby indicating that the QD immunoprobe that is blocked by BSA had few nonspecific adsorption of antibody, and few fluorescence resonance energy transfer (FRET) had happened between QD immunoprobe and fluorescence labeled on antibody. Meanwhile, the Cy5.5 labeled on antibody was almost not excited with a single laser (405 nm) at a wavelength far from its excitation wavelength.

When a 1 nM Cy5.5−2,4-D antibody solution and 2 nM QD immunoprobe was incubated for 5 min and was delivered to the microfluidic channel, however, a fluorescent signal was detected. As the concentration of fluorescence labeled antibody was increased to 10 nM, a signal-to-noise ratio (S/N, the ratio of the maximum fluorescent signal to the baseline) of >10 was obtained (Figure 3). These results showed that fluorescence-labeled anti-2,4-D antibody specially bound with the QD immunoprobe and the fluorescence signal detected originated from the QD-FRET.

To determinate the fluorescence energy transfer efficiency (E) in this system, the filter of the all-fiber biosensing platform was changed into a 605-nm bandpass filter (FF01-605/15, Semrock, USA). The energy transfer efficiency of QD immunoprobe with and without the presence of Cy5.5 labeled anti-2,4-D antibody is shown in Figure 4. The energy transfer

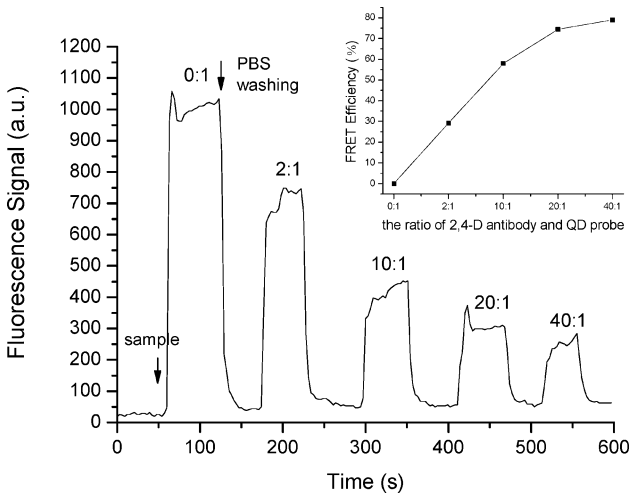

Figure 4. Emission fluorescence signal of QD donors at different acceptor-to-donor ratios (donor: QD/BSA/2,4-D; acceptor: fluorescence-labeled anti-2,4-D antibody). Inset shows the fluorescence resonance energy transfer (FRET) efficiency as a function of the acceptor-to-donor ratio. Each data value is the average of two independent experimental results.

efficiency (E) increases as the fluorecence-labeled antibody concentration increases. When the ratio between the antibody and the QD immunoprobe is >20, the value of E is estimated to be >78.4%, according to eq 1:[22]

$$E = 1 - \frac{F}{F_0} \quad (1)$$

where F and F_0 are, respectively, the QD (donor) fluorescences at 605 nm with and without the presence of Cy5.5 labeled 2,4-D antibody (acceptor). The FRET efficiency is strongly dependent on the separation distance between donors and acceptors, the spectral overlap of the donor emission spectrum and the acceptor absorption spectrum, and the relative orientation of the donor emission dipole moment and the acceptor absorption dipole moment.[5,6] Förster energy transfer is generally most efficient when the distance between donors and acceptors is in the range of 20−60 Å.[22] In our system, the center-to-center separation distances between the 605-nm QD donor and the Cy5.5 acceptor is >10 nm, assuming that the 2,4-D-BSA and the antibody are sequentially and perpendicularly attached on the QD surface and we account for the increased QD size (9−16 nm), which is due to the 2,4-D-BSA (3−4 nm)[23] and the antibody (6−10 nm).[23,24] However, our results demonstrated a high-efficiency FRET and a high sensitivity of the sensor for detecting specific binding between QD immunoprobe and anti-2,4-D antibody. We assumed that the following reasons contribute to the high FRET:

First, an ensemble of QD immunoprobes likely displays a heterogeneous mixture of multiple-hapten orientation and binding sites, because of the high ratio of 2,4-D attached to carrier protein (BSA); therefore, the

dx.doi.org/10.1021/ac3000495 | Anal. Chem. 2012, 84, 3646−3653

fluorescence-labeled antibody easily binds to the QD in various randon orientations, and some dyes are always in close proximity to the QD surface.

Second, the high number of hapten molecules attached to each carrier protein made it possible that several fluorescence-labeled antibodies can simultaneously bind to the QD surface, and several acceptor dyes interact with a single QD donor substantially, which consequently improves the FRET efficiency.[6] This was confirmed in the FRET data collected from experiments using increasing ratios of dye-labeled antibody per QD, where the measured efficiencies increased as the acceptor-to-donor ratios in each conjugate increased, as expected (see inset of Figure 4). In addition, the structure of the QD/BSA/2,4-D conjugate may avoid the steric hindrance, thus improving the antigen–antibody binding reaction.[20]

Binding Kinetics. We measured the immuno-reaction kinetics between QD immunoprobe and fluorescence-labeled anti-2,4-D antibody to determine the rate and amount of time required for the QD-based immunoassay to reach completion. First, 80 μL of the 2 nM QD immunoprobe was added into the sample cell, and 10 nM 2,4-D fluorescence labeled antibody was rapidly added and slightly stirred. As shown in Figure 5 (each

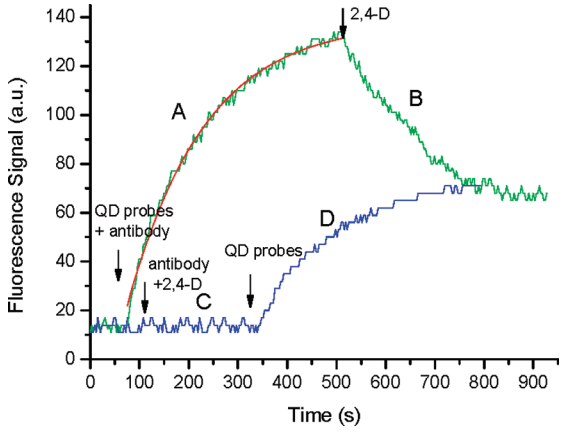

Figure 5. Assessing binding reaction kinetics and assay format by all-fiber biosensing platform. (A) A typical kinetic curve of molecular interaction, after short background measurement, the association phase is observed by introducing a 10 nM fluorescence-labeled antibody to 2 nM QD immunoprobe surface. Signal curve fits derived from first-order kinetics model were applied (red line). (B) 200 nM 2,4-D was introduced the mixture of antibody and QD immunoprobe; (C) 10 nM fluorescence-labeled antibdoy and 200 nM 2,4-D was introduced in sample cell; and (D) 2 nM QD was added into the mixture of antibody and 2,4-D solution.

curve being the average of three independent curves), real-time monitoring of the fluorescence signal can be carried out as the binding reaction occurring between the fluorescence-labeled antibody and QD immunoprobe, reflecting the reaction kinetics. The fluorescence signal exponentially increases over time due to FRET, and eventually reached a plateau after 8 min. This binding reaction curve seems to have first-order kinetics, and is fit to the equation (see the red line in Figure 5)

$$I(t) = A(1 - e^{-kt}) + b \quad (2)$$

where A is the pre-exponential weight, k the associated binding rate constant, and $I(t)$ the observed fluorescence intensity at time t. Our results show that the binding rate constant between the QD immunoprobe and the fluorescence-labeled antibody is 6.8×10^{-3} s^{-1}. We estimate that the binding reaction rate is at least 10–20 times faster than heterogeneous assays (e.g., ELISA, SPR), in which a complete binding reaction between an antibody and an antigen on flat surfaces requires hours instead of minutes.[25] We assume that the ability of nanoparticles to diffuse in solution and constantly refresh their depletion layer contributes to the faster kinetics in nanoparticle-based immunoassays.

Two assay formats were compared: fluorescence-labeled anti-2,4-D antibody and QD immunoprobe are first incubated and 2,4-D solution is then added, or fluorescence-labeled anti-2,4-D antibody and 2,4-D solution are first incubated and QD immunoprobe is then added. In the first assay format, when the fluorescence-labeled antibody was added into QD immunoprobe solution, the fluorescence signal increased over time and reached a plateau after ~8 min as curve A in the Figure 5. After the 2,4-D sample was added into the mixture, the fluorescence signal decreases over time and reached a new plateau after another 7 min, as depicted in curve B in Figure 5. In the other one, when the fluorescence-labeled antibody and 2,4-D solution were mixed in the sample cell, few fluorescence signals could be observed (curve C in Figure 5). Once the QD immunoprobe was added into the mixture, the fluorescence signal increased with over time and eventually reached a plateau after ~7 min, as depicted in curve D in Figure 5. Curves B and D in Figure 5 show that the fluorescence signal values of two assay formats at the equilibrium state were basically constant. These results showed that free 2,4-D in solution and haptens immobilized onto the QD surface might competitively bind with the fluorescence-labeled antibody and the final result was not affected, regardless of the assay formats that were applied. The reason is that the equilibrium constant is the major limiting factor of fractionation between the antigen and the antibody, because of the law of mass action in competitive assays.[26] Therefore, in all the following experiments, the 2,4-D sample, QD immunoprobe, and fluorescence-labeled antibody were incubated simultaneously for 8 min and then introduced into the microfluidic channel for 2,4-D detection.

Immunoassay Mechanism. Figure 1c illustrates the competitive immunoassay mechanism for small molecular analytes based on QD-FRET. During one detection cycle, 2,4-D solutions of different concentrations, the fluorescence-labeled antibody and QD immunoprobe of a fixed concentration were mixed and incubated for 8 min. During incubation, both the free 2,4-D (analyte) in solution and antigens immobilized onto the QD immunoprobe surface competitively bind simultaneously with the fluorescence-labeled antibodies. The higher the concentration of 2,4-D, the less antibodies bind with the QD immunoprobe and, therefore, the lower the resultant fluorescence signal. Once the equilibrium state of this competitive antigen–antibody reaction was reached, the mixture was introduced into the microfluidic channel and the fluorescence signal was detected by the all-fiber microfluidic biosensing platform.

Optimization of Competitive Immunological Reaction. Once the detection platform, immunoassay mechanism, assay format, and assay time are established, optimization of the reagent concentrations is the next step to improve the sensitivity of the assay. With the aim of selecting the best concentration of QD immunoprobe and fluorescence labeled antibody, a checkerboard titration was run with a serials of

dx.doi.org/10.1021/ac3000495 | Anal. Chem. 2012, 84, 3646–3653

dilution for various combinations, as shown in Figure 6a. The results showed that, for a certain concentration of QD

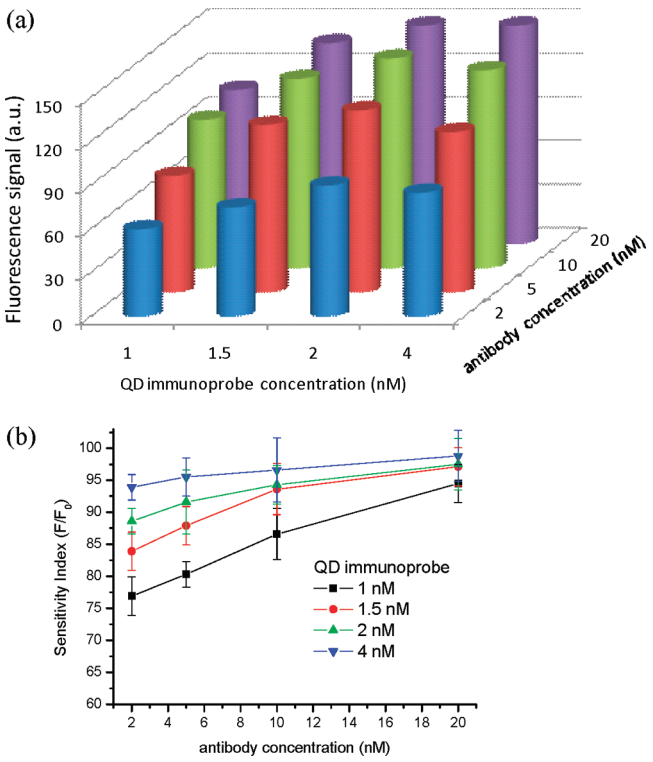

Figure 6. (a) Experimental optimization of the QD immunoprobe and the fluorescence-labeled antibody concentration ,using the checkerboard titration; (b) the sensitivity index (F/F_0) was calculated from the fluorescence intensity with 10 nM 2,4-D (F) and in the absence of target antigen (F_0). The error bars correspond to the standard deviations of the data points in triplicate experiments.

immunoprobe, the fluorescent signal increased as the concentration of fluorescence-labeled antibody increased and then reached a plateau. The higher concentration of fluorescence-labeled antibody may lead to more antibodies being bound to the QD immunoprobe and, therefore, the higher the resultant fluorescence signal. The reason is that binding more acceptor dyes to one QD surface obviously improves the FRET efficiency.[6] On the other hand, as the QD immunoprobe concentration increases, the fluorescence signal detected increases when the concentration of QD immunoprobe was <2 nM. However, the fluorescence intensity detected when the QD immunoprobe is 4 nM increases as the antibody concentration increases, but was slightly less than that detected when the QD immunoprobe is 2 nM. We assumed that, as the QD immunoprobe concentration increases, each of them binds to fewer fluorescence-labeled antibodies, and the number of antibodies close to the QD immunoprobe surface may decrease, because the direction of the haptens immobilized onto carrier protein is anisotropic, which results in a decrease in FRET efficiency.

To determine the optimum experimental conditions, a sensitivity index (F/F_0), which is defined as the ratio between the fluorescence intensity obtained in the presence of the analyte (F) and that in the absence of analyte (F_0), was introduced. In this paper, the sensitivity index was calculated from the fluorescence intensity with 10 nM 2,4-D (F) and in the absence of target antigen (F_0). For the practical application of the sensor, the most acceptable QD immunoprobe and 2,4-D antibody concentration were chosen according to the following criteria: (1) the S/N ratio (the ratio of the maximum fluorescent signal to the baseline) should be as high as possible, and preferably >10, in order to generate a reasonable QD fluorescence intensity; and (2) the sensitivity index should be as low as possible, and preferably <0.95 to be suitable for the desired dynamic range in practical applications. Based on these criteria, several experiments were conducted (Figure 6b) and the best pair of sensing elements was as follows: QD immunoprobe = 1.5 nM, and fluorescence-labeled antibody = 5 nM. Lower concentrations of reagents (QD immunoprobe and fluorescence-labeled antibody) are beneficial for the effective competition of analyte in a competitive immunoassay, which will result in better sensitivity.

Dose–Response Measurements of 2,4-D. Once the general assay parameters have been optimized, 2,4-D standard solutions in the range of 0–30 μM were explored to verify the competitive fluorescence immunoassay. Figure 7a show the temporal fluorescence signal during a typical test cycle for 2,4-D detection using the all-fiber microfluidic biosensing platform developed here, including the introduction of a mixture of the

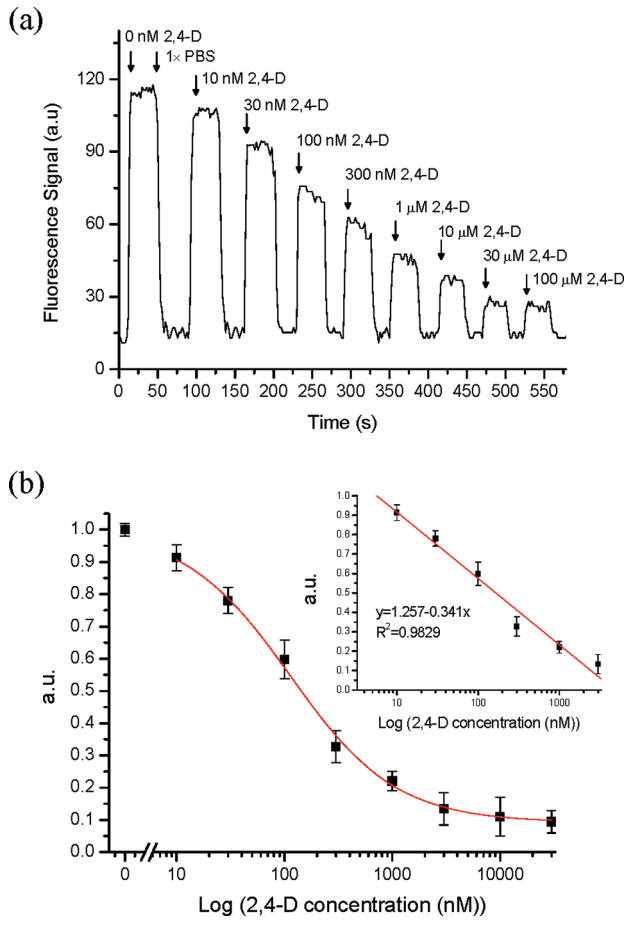

Figure 7. Competitive immunoassay of 2,4-D. (a) Signal traces observed as the mixture of 5 nM fluorescence-labeled antibody, 1.5 nM QD immunoprobe, and 2,4-D solutions of various concentrations flow over the microfluidic channel. (b) Dose–response curves as the normalized values, expressing the signal of each standard point as the ratio to that of the blank sample containing no 2,4-D. Inset indicates the dynamic range, showing the linear relationship between the 2,4-D concentration and fluorescence intensity.

dx.doi.org/10.1021/ac3000495 | Anal. Chem. 2012, 84, 3646–3653

fluorescence-labeled antibody, the QD immunoprobe and sample, and a washing step. One can see that the introduction of 2,4-D at different concentrations to the mixture induced proportional decreases in the fluorescence signal. As seen in Figure 7b, the proportionally decreasing signal as the concentration of 2,4-D was increased established a dose–response curve (each being the average of three independent curves) for the detection of 2,4-D over a concentration range from 0.5 μM to 30 μM. The detection limits of 0.5 nM for 2,4-D were obtained from the calibration curve based on a S/N ratio of 3. The quantification of 2,4-D over concentration ranges from 0 to 3 μM, with a relative standard deviation, as a percentage (%RSD), in the range of 1.25%–5.89%. The detection limit observed is approximately several orders of magnitude lower than those of the electrochemical impedance measurements (500 nM)[27] and conventional ELISA (2 μM),[28] and is comparable to that of the SPR (4.5 nM).[20] Higher sensitivity detection of 2,4-D (0.1 nM) has been achieved some immunoassay methods based on chemiluminescence or fluorescence,[29,30] and a QCM-based immunosensor was shown to exhibit a very low detection limit of 0.05 nM.[31] Compared to these sensors, however, that which has been developed here is much simpler, and faster (only 6 min, including measurement and regeneration), which results from the dynamic binding interaction between antibody and QD immunoprobe. In addition, without any loss in sensitivity, the dimensions of microfluidic device ensures a total volume (~35 μL) less than that of conventional ELISA requiring at least 100 μL to be filled in microwell,[25] which greatly reduces the assay cost, because some reagents are very expensive.

To the best of our knowledge, this is the first time such a high sensitivity is reported for the detection of 2,4-D employing QD-FRET. By essembling a carrier–proteins/haptens conjugate onto QD surfaces, several unique advantages over those probes prepared by immobilizing antibody onto QD surface for FRET sensor became apparent. First, 2,4-D-BSA conjugates used as recognition elements were covalently attached to the QD surface as immunoassay probes with a EDC/NHS chemistry, which could prevent the compromise of the binding properties of immobilized biomolecules, and the binding sites of the QD immunoprobe can avoid the steric hindrance and keep highly active for its antibody. Second, QD/carrier–protein/haptens conjugate as a detection probe is more stable in complex environmental samples than typical biorecognition molecules in biosensor, such as antibody, enzymes, protein, and live microbes. Third, the FRET efficiency is higher due to more acceptor dyes bound to one QD surface, which enables the QD-FRET assay to offer high sensitivity. In addition, the QD immunoprobe prepared herein can be stored over two months with little significant deterioration (<15%) of performance (see Figure S-4 in the Supporting Information).

Selectivity of Nanosensor. To investigate potential interference from other environmental pollutants which have closely resembling structure with 2,4-D, we evaluated the sensor's response to two carcinogenic environmental toxics (2,4,5-T and 2,4-DCP) and three others (2,4-DB, CPA, and MCPA). The sensor exhibits high selectivity toward 2,4-D with no significant response (<12%, as comparable to a blank control) to the other ,closely resembling environmental pollutants (see Figure S-5 in the Supporting Information). This selectivity must be due to the specificity of the antibody, which is an important factor when analyzing environmental samples on-site without separation.

Spiked Environmental Water Samples Analysis. To study the influence of matrix effect on QD-FRET-based nanobiosensor response, several samples spiked with 2,4-D, with concentration grades of 20 nM, 200 nM, and 1000 nM, were tested by spiking the filtered water samples. All samples were measured unspiked to ensure that they were not contaminated (<0.5 nM). The results are summarized in Table 1. The recovery of all measured samples was 90%–105%, and the parallel tests showed that the coefficient of variation was <7% (n = 3). These data confirm that the proposed sensing system based on QD-FRET is applicable for 2,4-D detection with sufficient precision and accuracy, even in real environmental sample matrices.

Table 1. Sample Set of Results Showing Recoveries of Analyte from Four Different 2,4-D-free Water Samples (Bottled water, Tap water, Advanced treatment effluent water, and Lake water) spiked with three analyte concentrations

	%Recovery[a]			
concentration of 2,4-D (nM)	bottled water	tap water	advanced treatment effluent water	lake water
0	95(1.09)	102(3.38)	94(5.03)	102(6.21)
20	96(3.09)	94(4.19)	93(3.78)	97(3.02)
200	101(2.02)	98(2.09)	96(3.97)	95(3.45)
1000	93(3.12)	103(2.04)	91(5.09)	97(2.08)

[a]%Recovery was calculated for the negative control and three standard concentrations as follows: %Recovery = (quantity measured/quantity expected) × 100. All water samples were collected in October 2011 and pretreated using a 0.22-μm syringe filter to exclude the interference effect caused by particles. The values in parentheses indicate the coefficient of variance (%CV), based on three replicate experiments.

CONCLUSION

A quantum dot–fluoresence resonance energy transfer (QD-FRET)-based nanoimmunosensor has been successfully developed for the detection of 2,4-D using QD/BSA/2,4-D conjugate as a detection probe. The structure of a multiplex–haptens/BSA conjugate coupling to the QD greatly improves the FRET efficiency. Base on the competitive immunoassay mode, the biosensing assay of 2,4-D using the homemade all-fiber microfluidic biosensing platform in water samples featured good characteristics with its high sensitivity, rapidity, and ease of use. While 2,4-D was chosen as the model, with the use of different QD immunoprobes modified by the conjugates of other haptens/carried protein, the methodology presented here has the potential to extend toward the on-site monitoring of other small analytes in a variety of application fields ranging from environmental to biochemical areas.

ASSOCIATED CONTENT

Supporting Information

Additional information as noted in text. This material is available free of charge via the Internet at http://pubs.acs.org.

AUTHOR INFORMATION

Corresponding Author

*E-mail: hanchang@tsinghua.edu.cn.

Notes

The authors declare no competing financial interest.

■ ACKNOWLEDGMENTS

This research was financially supported by the National Natural Science Foundation of China (No. 21077063), the 863 National High Science and Technology Development Programs of China (No. 2009AA06A417-07), and the Supervisor's Project of Outstanding Doctoral Dissertation Award of Beijing (No. YB20091000302).

■ REFERENCES

(1) Bernard, A.; Hermans, C.; Broeckaert, F.; De Poorter, G.; De Cock, A.; Houins, G. *Nature* **1999**, *401*, 231−232.
(2) Adams, A. A.; Charles, P. T.; Deschamps, J. R.; Kusterbeck, A. W. *Anal. Chem.* **2011**, *83*, 8411−8419.
(3) Zhu, Z.; Ravelet, C.; Perrier, S.; Guieu, V.; Roy, B.; Perigaud, C.; Peyrin, E. *Anal. Chem.* **2010**, *82*, 4613−4620.
(4) Agasti, S. S.; Rana, S.; Park, M.; Kim, C. K.; You, C.; Rotello, V. M. *Adv. Drug Delivery Rev.* **2010**, *62*, 316−328.
(5) Medintz, I. L.; Clapp, A. R.; Mattoussi, H.; Goldman, E. R.; Fisher, B.; Mauro, J. M. *Nat. Mater.* **2003**, *2*, 630−638.
(6) Algar, W. R.; Tavares, A. J.; Krull, U. J. *Anal. Chim. Acta* **2010**, *673*, 1−25.
(7) Kuo, Y.; Wang, Q.; Ruengruglikit, C.; Yu, H.; Huang, Q. *J. Phys. Chem. C* **2008**, *112*, 4818−4824.
(8) Yu, X.; Chen, L.; Li, K.; Li, Y.; Xiao, S.; Luo, X.; Liu, J.; Zhou, L.; Deng, Y.; Pang, D.; Wang, Q. *J. Biomed. Opt.* **2007**, *12*, 1−5.
(9) Jaiswal, J. K.; Mattoussi, H.; Mauro, J. M.; Simon, S. M. *Nat. Biotechnol.* **2003**, *21*, 47−51.
(10) Yong, K. T.; Ding, H.; Roy, I.; Law, W. C.; Bergey, E. J.; Maitra, A.; Prasad, P. N. *ACS Nano* **2009**, *3*, 502−510.
(11) Rosenthal, S. J.; Chang, J. C.; Kovtun, O.; McBride, J. R.; Tomlinson, I. D. *Chem. Biol.* **2011**, *18*, 10−24.
(12) Medintz, I. L.; Goldman, E. R.; Lassman, M. E.; Mauro, J. M. A. *Bioconj. Chem.* **2003**, *14*, 909−918.
(13) Goldman, E. R.; Balighian, E. D.; Mattoussi, H.; Kuno, M. K.; Mauro, J. M.; Tran, P. T.; Anderson, G. P. *J. Am. Chem. Soc.* **2002**, *124*, 6378−6382.
(14) Medintz, I. L.; Konnert, J. H.; Clapp, A. R.; Stanish, I.; Twigg, M. E.; Mattousssi, H.; Mauro, J. M.; Deschamps, J. R. *Proc. Natl. Acad. Sci. U.S.A.* **2004**, *121*, 9612−9617.
(15) Barzen, C.; Brecht, A.; Gauglitz, G. *Biosens. Bioelectron.* **2002**, *17*, 289−295.
(16) Ibrahim, M. A.; Bond, G. G.; Burkee, T. A.; Cole, P.; Dost, F. N.; Enterline, P. E.; Gough, M.; Greenberg, R. S.; Halperin, W. E.; McConnell, E.; Munro, I. C.; Swenberg, J. A.; Zahm, S. H.; Graham, J. D. *Environ. Health Perspect.* **1991**, *96*, 213−222.
(17) Sheiner, E. K.; Sheiner, E.; Hammel, R. D.; Potashnik, G.; Carel, R. *Ind. Health* **2003**, *41*, 55−62.
(18) Burns, C. J.; Beard, K. K; Cartmill, J. B. *Occup. Environ. Med.* **2001**, *58*, 24−30.
(19) Long, F.; Shi, H. C.; He, M.; Zhu, A. N. *Biosens. Bioelectron.* **2008**, *23*, 1361−1366.
(20) Gobi, K. V.; Kima, S. J.; Tanaka, H.; Shoyamac, Y.; Miura, N. *Sens. Actuators B* **2007**, *123*, 583−593.
(21) Chi, C. W.; Lao, Y. H.; Li, Y. S.; Chen, L. C. *Biosens. Bioelectron.* **2011**, *26*, 3346−3352.
(22) Lakowicz, J. R. *Principles of Fluorescence Spectroscopy*, 2nd Edition; Kluwer Academic, New York. 1999.
(23) Murphy, R. M.; Slayter, H.; Schurtenberger, P.; Chamberlin, R. A.; Colton, C. K.; Yarmush, M. L. *Biophys. J.* **1988**, *54*, 45−56.
(24) Yarmush, D. M.; Murphy, R. M.; Colton, C. K.; Fisch, M.; Yarmush, M. L. *Mol. Immunol.* **1988**, *25*, 17−25.
(25) Lim, C. T.; Zhang, Y. *Biosens. Bioelectron.* **2007**, *22*, 1197−1204.
(26) Zhuang, G.; Katakura, Y.; Omasa, T.; Kishimoto, M.; Suga, K. *J. Biosci. Bioeng.* **2001**, *92*, 330−336.
(27) Navaratilova, I.; Skladal, P. *Bioelectrochemistry* **2004**, *62*, 11−18.
(28) Tanaka, H.; Yan, S.; Miura, N.; Shoyama, Y. *Cytotechnology* **2003**, *42*, 101−107.
(29) Sanchez, F. G.; Diaz, A. N.; Diaz, A. F. G.; Eremin, S. A. *Anal. Chim. Acta* **1999**, *378*, 219−224.
(30) Danielsson, B.; Surugiu, I.; Dzgoev, A.; Mecklenburg, M.; Ramanathan, K. *Anal. Chim. Acta* **2001**, *426*, 227−234.
(31) Svitel, J.; Dzgoev, A.; Ramanathan, K.; Danielsson, B. *Biosens. Bioelectron.* **2000**, *15*, 411−415.